Published in final edited form as:
J Neurosurg. 2011 May ; 114(5): 1319–1330. doi:10.3171/2010.11.JNS10768.

The neurosurgical anatomy of the sphenoid sinus and sellar floor in endoscopic transsphenoidal surgery

Gabriel Zada, M.D.[1], **Pankaj K. Agarwalla, M.D.**[2], **Srinivasan Mukundan Jr., Ph.D., M.D.**[3], **Ian Dunn, M.D.**[4], **Alexandra J. Golby, M.D.**[4], and **Edward R. Laws Jr., M.D.**[4]

[1]Department of Neurosurgery, Keck School of Medicine, University of Southern California, Los Angeles, California

[2]Department of Neurosurgery, Massachusetts General Hospital, Harvard Medical School, Boston, Massachusetts

[3]Division of Neuroradiology, Brigham and Women's Hospital, Harvard Medical School, Boston, Massachusetts

[4]Department of Neurosurgery, Brigham and Women's Hospital, Harvard Medical School, Boston, Massachusetts

Abstract

Object—A considerable degree of variability exists in the anatomy of the sphenoid sinus, sella turcica, and surrounding skull base structures. The authors aimed to characterize neuroimaging and intraoperative variations in the sagittal and coronal surgical anatomy of healthy controls and patients with sellar lesions.

Methods—Magnetic resonance imaging studies obtained in 100 healthy adults and 78 patients with sellar lesions were reviewed. The following measurements were made on midline sagittal images: sellar face, sellar prominence, sellar angle, tuberculum sellae angle, sellar-clival angle, length of planum sphenoidale, and length of clivus. The septal configuration of the sphenoid sinus was classified as either simple or complex, according to the number of septa, their symmetry, and their morphological features. The following measurements were made on coronal images: maximum width of the sphenoid sinus and sellar face, and the distance between the parasellar and midclivus internal carotid arteries. Neuroimaging results were correlated with intraoperative findings during endoscopic transsphenoidal surgery.

Results—Three sellar floor morphologies were defined in normal adults: prominent (sellar angle of < 90°) in 25%, curved (sellar angle 90–150°) in 63%, flat (sellar angle > 150°) in 11%, and no

Address correspondence to: Gabriel Zada, M.D., USC Department of Neurosurgery, 1200 North State Street, Suite 5046, Los Angeles, California 90089. gzada@usc.edu.

Disclosure

The authors report no conflict of interest concerning the materials or methods used in this study or the findings specified in this paper.

Author contributions to the study and manuscript preparation include the following. Conception and design: Zada, Mukundan, Dunn, Golby, Laws. Acquisition of data: Zada, Agarwalla. Analysis and interpretation of data: Zada, Agarwalla, Mukundan, Dunn, Laws. Drafting the article: Zada, Golby, Laws. Critically revising the article: Agarwalla, Mukundan, Dunn, Golby, Laws. Reviewed final version of the manuscript and approved it for submission: all authors. Statistical analysis: Zada, Agarwalla. Administrative/technical/material support: Mukundan, Dunn, Golby. Study supervision: Mukundan, Golby, Laws.

floor (conchal sphenoid) in 1%. In healthy adults, the following mean measurements were obtained: sellar face, 13.4 mm; sellar prominence, 3.0 mm; sellar angle, 112°; angle of tuberculum sellae, 112°; and sellar-clival angle, 117°. Compared with healthy adults, patients with sellar lesions were more likely to have prominent sellar types (43% vs 25%, $p = 0.01$), a more acute sellar angle (102° vs 112°, $p = 0.03$), a more prominent sellar floor (3.8 vs 3.0 mm, $p < 0.005$), and more acute tuberculum (105° vs 112°, $p < 0.01$) and sellar-clival (105° vs 117°, $p < 0.003$) angles. A flat sellar floor was more difficult to identify intraoperatively and more likely to require the use of a chisel or drill to expose (75% vs 25%, $p = 0.01$). A simple sphenoid sinus configuration (no septa, 1 vertical septum, or 2 symmetric vertical septa) was noted in 71% of studies, and the other 29% showed a complex configuration (2 or more asymmetrical septa, 3 or more septa of any kind, or the presence of a horizontal septum). Intraoperative correlation was more challenging in cases with complex sinus anatomy; the most reliable intraoperative midline markers were the vomer, superior sphenoid rostrum, and bilateral parasellar and clival carotid protuberances.

Conclusions—Preoperative assessment of neuroimaging studies is critical for characterizing the morphological characteristics of the sphenoid sinus, sellar floor, tuberculum sellae, and clivus. The flat sellar type identified in 11% of people) or a complex sphenoid sinus configuration (in 29% of people) may make intraoperative correlation substantially more challenging. An understanding of the regional anatomy and its variability can improve the safety and accuracy of transsphenoidal and extended endoscopic skull base approaches.

Keywords

sphenoid sinus; sella turcica; tuberculum sellae; clivus; transsphenoidal approach; pituitary gland

---

The transsphenoidal approach has evolved considerably since it was first successfully performed by Schloffer in 1907 and is currently the gold standard approach for many lesions of the pituitary gland and parasellar region.[6,12] In recent decades, the operating microscope and endoscope have greatly facilitated the visualization associated with this approach, and related extended endonasal approaches, for a wide spectrum of skull base pathologies. In the majority of cases, the approach to the sella is facilitated by the identification of key anatomical landmarks including the vomer, sellar floor, sphenoid rostrum, clivus, tuberculum sellae, and OCRs. A remarkable degree of anatomical variation, however, exists in the sphenoid sinus, sella turcica, and surrounding anterior and central skull base structures, at times making the transsphenoidal approach more challenging and less advantageous.[9] One of the primary considerations during any endonasal transsphenoidal operation is maintaining constant awareness of the midline, to avoid inadvertent injury to critical paramedian structures, such as the ICA, cavernous sinus, and optic nerves. In the majority of cases, intraoperative identification of the sellar midline and paramedian anatomy proceeds without significant challenge to the surgeon. In some patients with complex sellar anatomy, nonpneumatized sphenoid sinuses, or those undergoing reoperation, however, the typical appearance of the sella turcica and its relationship to the tuberculum sellae and clivus may be less conspicuous, and identification of the midline is often more challenging, substantially increasing the risk of the operation.[2]

Although advances in endoscopic approaches and intraoperative neuronavigation have improved the visualization and accuracy associated with transsphenoidal and related

extended endonasal skull base surgery over the last decade, they by no means obviate the requirement for knowledge and a thorough preoperative assessment of the relevant surgical anatomy on neuroimaging studies. Because of normal anatomical variations of the sellar region and the effects that tumor growth and expansion have on the regional anatomy, a thorough assessment of preoperative neuroimaging studies is imperative prior to performing any transsphenoidal operation. Successful correlation of intraoperative anatomical findings with preoperative neuroimaging features maximizes the safety of any endonasal skull base approach.

In 1961, Hamberger et al.[5] described 3 anatomical variations of the sphenoid sinus (sellar, presellar, and conchal) that are still in use today. Since that time, several cadaveric and radiographic studies have examined the anatomical variations of the sphenoid sinus and its relationship to the sella turcica.[7,9,11,13,15] Few studies, however, have analyzed these anatomical patterns with regard to imaging-intraoperative correlation in healthy individuals and patients with sellar lesions during the modern era of neuroimaging and endoscopic surgery. Although CT imaging is typically the preferred modality for the assessment of bony skull base anatomy, we aimed to assess the spectrum of normal and pathological variation in sellar and parasellar surgical anatomy based on MR imaging, because MR imaging remains the gold standard for characterizing pathology of the sellar region and is the preferred modality for intraoperative neuronavigation at many institutions.

In the current study, we aimed to characterize variations in sellar and parasellar anatomy based on MR imaging, both in healthy adults and in patients undergoing transsphenoidal operations, followed by an assessment of the ability to achieve intraoperative anatomical correlation with these imaging studies. Furthermore, the importance of reviewing sinus and sellar floor anatomy before tailoring a particular approach and deciding on its extent, guiding the discussion of operative risks with the patient preoperatively, and gauging the need for additional instrumentation and/or intraoperative neuronavigation, is discussed.

Methods

Following approval by the institutional review board, noncontrast sagittal T1-weighted MR imaging studies were reviewed in 100 healthy adults (50 men and 50 women) with no known sellar pathology. All measurements were performed independently by 2 reviewers and confirmed by a staff neuroradiologist. For coronal imaging, specialized thin-cut, reformatted coronal T1-weighted spoiled gradient recall sequence (3-T MR imaging) studies were then reviewed in 78 healthy adult volunteers with no known sellar pathology (Vitrea FX by Vital Images) as part of a neuroimaging research protocol at Brigham and Women's Hospital. The preoperative MR imaging studies and operative records of 154 patients undergoing transsphenoidal surgery for sella-based lesions at Brigham and Women's Hospital between April 2008 and July 2009 were subsequently reviewed (Centricity Enterprise v3.0, GE Medical Systems, 2006). Patients with previous transsphenoidal surgery and those with imaging or intraoperative evidence of infrasellar extension into the sphenoid sinus were excluded from the study, and 78 patients were included in the analysis.

For each study, measurements of the sellar and sphenoid sinus anatomy were made using computer-based imaging software. The following measurements were obtained on midline sagittal images (Fig. 1): sellar face, defined as the distance from the tuberculum sellae to the sellar-clival point; sellar prominence, defined as the longest perpendicular distance from the tuberculum-clival line to the most prominent point on the sellar floor convexity; length of the planum sphenoidale within the sphenoid sinus; clival length (shortest linear distance from the sellar-clival point to the sphenoid sinus floor); sellar angle (angle between lines drawn tangential to the sellar floor at the tuberculum sellae and sellar-clival points); angle of the tuberculum sellae; and sellar-clival angle. Following analysis of these initial anatomical data, 3 sellar types were defined based on the sellar angle and convexity: prominent sella (sellar angle < 90°), curved sella (sellar angle 90°–150°), and flat sella (sellar angle > 150°) (Fig. 2).

The following measurements were then obtained from coronal imaging sequences: number and posterior origin of vertical sphenoid sinus septations, number of horizontal sphenoid sinus septations, maximum width of the sphenoid sinus (excluding inferolateral recesses), width of the sellar face (anteriorly between the medial cavernous sinus walls), distance between the intercavernous parasellar ICAs, and distance between the ICAs at the midclivus. Symmetry or asymmetry of the sinus was also noted.

Based on the number of sphenoid sinus septations and the overall symmetry of the sinus with respect to the vertical midline, a classification scheme of “simple” or “complex” sphenoid morphology was created. Simple sphenoid sinus septation patterns included several subtypes: no septations, 1 vertical septation (midline or eccentric), or 2 symmetrical vertical septations creating a tripartite sinus. Patients were considered to have complex sphenoid sinus morphology if they had 2 asymmetrical vertical septations, 3 or more septations of any type, or any horizontal septations. Intraoperative observations pertaining to these imaging studies were then made in 22 patients undergoing endoscopic transsphenoidal operations with the use of intraoperative MR imaging neuronavigation. The frequency with which the sellar floor was easily identifiable was noted, as was the frequency with which each of the following structures could be used to identify the sellar midline: base of the vomer, superior rostrum of the sphenoid, OCRs, parasellar carotid protuberances, and clival-carotid prominences. Data were analyzed using an unpaired t-test to compare means and a Fisher exact test to compare categorical data (GraphPad, Inc.). Statistical significance was defined as a probability value < 0.05.

Operative Technique

The standard endoscopic approach to the sella turcica and pituitary gland has been described at length elsewhere.[1] The majority of surgical cases were performed via an endoscopic transsphenoidal approach, with intraoperative MR imaging–based neuronavigation (BrainLab) available in all cases. Once the sellar floor and surrounding structures were identified, an attempt was typically made initially to fracture the floor with a blunt nerve hook if the floor appeared thin enough. In the case of a thicker sellar floor, a chisel or drill is used for the initial dural exposure. The exposure of the sellar dura then proceeds using a

Kerrison rongeur, nerve hook, and/or drill. Intraoperative Doppler ultrasonography is used in the majority of cases to detect the intracavernous ICA prior to opening the dura.

Results

Sagittal MR Anatomy of the Sella Turcica in Healthy Adults

The results following analysis of neuroimaging studies in healthy adults are presented in Table 1. The mean length of the sellar face (tuberculum sella to sellar-clival point) was 13.4 mm (range 6.7–19.8 mm). The mean sellar prominence was 3 mm (range –1 to 6.5 mm). The mean length of the planum sphenoidale was 14.1 mm (range 6.4–28.8 mm). The mean clivus length below the sella was 14.6 mm (range 5.5–22.7 mm). The mean angle of the tuberculum sellae was 112° (range 70°–154°). The mean sellar-clival angle was 117° (range 65°–183°). The mean sellar angle was 112° (range 71°–180°).

The healthy adults were found to have the following sellar floor types (Fig. 2): prominent sella (< 90°) in 25% of individuals, curved sella (90°–150°) in 63%, flat sella (> 150°) in 11%, and conchal (no identifiable floor) in 1% (Fig. 3). Of the 11 patients with a flat sellar floor, 7 (64%) had a “presellar” type of sphenoid sinus.

Although there was a trend toward a more prominent sellar configuration in men (110°, 3.2 mm) compared with women (115°, 2.7 mm), this difference did not reach statistical significance. The only significant differences between men and women were a longer planum sphenoidale (15.1 vs 13.0 mm, $p = 0.012$) and a longer clivus length, as measured from within the sphenoid sinus (15.5 vs 13.6 mm, $p = 0.005$) in men.

Sellar Floor Anatomy in Patients With Intrasellar Lesions

Significant differences in sellar floor anatomy were noted between patients with sellar lesions and healthy adults (Table 2). On average, patients with sellar pathology had a longer sellar face than healthy adults (15.4 vs 13.4 mm, $p < 0.0001$), more prominent sellar floor (3.8 vs 3.0 mm, $p < 0.0036$), a more acute tuberculum sellae angle (105° vs 112°, $p < 0.0058$), and a more acute sellar-clival angle (105° vs 117°, $p < 0.003$), all features that are consistent with sellar expansion. The mean sellar angle in tumor patients was 102° compared with 112° in healthy individuals ($p = 0.03$). In patients with macroadenomas, the mean sellar angle was 99° ($p < 0.01$ in comparison with healthy adults).

Patients with intrasellar lesions were more likely to have a prominent sella turcica than were healthy adults (43% vs 25%, $p = 0.0163$) (Table 3). The proportion of patients with a prominent sellar floor was even greater in the group of patients with macroadenomas (45% vs 25%, $p = 0.0119$) (Figs. 4 and 5). No statistically significant difference was noted between healthy adults and patients with microadenomas.

Morphological Configuration of the Sphenoid Sinus in Healthy Adults and Patients

Results obtained following a review of coronal MR imaging studies in 100 healthy adults and 78 patients are presented in Table 4. A simple sphenoid sinus septum morphology was evident in 71% of studies (Fig. 6), and a complex sinus pattern in 29% (Fig. 7). The most common anatomical subtype was 1 eccentric vertical septum, identified in 34% of studies.

The presence of only 1 septum located directly in the midline was identified in 19% of imaging studies. The presence of 2 vertical septations creating a symmetric tripartite sinus was identified in 9%. Considering all vertical septations collectively, the posterior sphenoid sinus origin was midline in 47%, left posterior sinus near the ICA in 40%, and right posterior sinus near the ICA in 39% of studies. A thick bony "pillar" continuous with the lateral sinus wall was observed in 5% of patients, and an Onodi (posterior ethmoidal) air cell was identified in 3% of patients (all with horizontal and vertical septations and a complex sphenoid subtype). The vomer was located in the midline in all studies.

Coronal MR Imaging Measurements in Healthy Adults and Patients With Sellar-Region Lesions

In healthy adults, the mean maximum sphenoid sinus width was 30.1 mm (range 18.6–36.6 mm) (Table 5). The mean width of the sellar face was 12.7 mm (range 8.0–16.9 mm). The mean distance between the parasellar ICAs in cavernous sinus was 16.2 mm (range 7.4–25.5 mm), and the mean distance between the ICAs at the midclivus level was 18.5 mm (range 13.8–24.6 mm).

Compared with healthy adults, patients with intrasellar lesions were noted to have a wider sphenoid sinus (mean width 30.1 vs 31.4 mm, $p = 0.047$), wider sellar face (12.7 vs 15.9 mm, $p < 0.0001$), and a wider separation between the parasellar ICAs (16.2 vs 19.0 mm, $p < 0.0001$) (Table 5 and Fig. 8). In comparing findings in healthy adults with those in patients with lesions less than 10 mm in maximum diameter, only sellar face width showed a statistically significant difference (12.7 vs 14.2 mm, $p = 0.0008$) (Table 6). In comparing patients with smaller-diameter lesions (< 10 mm) to those with larger lesions (≥ 10 mm), differences were noted in the mean maximum sphenoid sinus width (29.2 vs 32.7 mm, $p = 0.0012$), sellar face width (14.2 vs 16.8 mm, $p < 0.0001$), and distance between parasellar ICAs (16.8 vs 20.2 mm, $p < 0.0001$) (Table 7). No statistically significant differences were noted in the separation between midclival ICAs among any groups.

Intraoperative Correlation

Intraoperative identification of the sellar floor was easier in patients with a prominent sellar morphology (14 of 14 patients) than in patients with a curved or flat sellar floor (3 of 8 patients). Intraoperative neuronavigation or intraoperative fluoroscopy provided a significant benefit in identifying the sellar face in the majority of cases (5 of 8) with a flat sellar type, yet was required primarily for confirmation in patients with a prominent sellar type (Fig. 9). In the majority of patients (75%) with a prominent sellar morphology, the floor was thin and could be easily fractured using a blunt nerve hook, compared with only 25% of patients ($p = 0.0157$) with a flat sella (Table 8). In the remaining 75% of patients with a flat sella, the sellar floor was thicker and required a chisel or drill for exposure.

Of the 22 patients studied intraoperatively, 18 (82%) had a simple type of sphenoid sinus pattern, and 4 (18%) had a complex type. Intraoperative findings/imaging correlation of vertical sphenoid sinus septations was achievable in all 22 patients, and was considerably easier to achieve in patients with simple patterns (Fig. 10). In patients with complex anatomy, the use of intraoperative neuronavigation and frequent reference to other midline

structures proved to be beneficial. In 11 patients (50%), vertical septations originated in the midline posteriorly, and served as useful midline markers. Lateral septae frequently originated posteriorly near the carotid protuberances. The base of the vomer and superior rostrum of the sphenoid were the most universal indicators of the midline and were identifiable in all patients (Fig. 11). A distinct sellar curvature and prominent sella was evident in 14 of 22 patients, facilitating identification of the sellar midline. The parasellar carotid protuberances served as distinct bilateral markers in 11 of 22 patients, from which the location of the midline could usually be extrapolated (Fig. 12). The identification of well-pneumatized bilateral OCRs was possible in only 4 of 22 cases, although for typical (nonextended) approaches to the sella, identification of the OCRs is not actively pursued. Finally, distinct bilateral clival-carotid prominences were identifiable in 10 of 22 cases.

Discussion

A substantial degree of anatomical variation exists in the sella turcica, sphenoid sinus, and adjacent anterior and central skull base structures. In 1961, Hamberger et al.[5] provided the original classification of the sphenoid sinus as it relates to the sellar floor, and this classification is still useful. Several studies have reported findings regarding the observed proportions of each of these anatomical variations: a normal “sellar” sinus (80%–86%), a “presellar” variety with minimal pneumatization of the sinus (10%–20%), and a conchal variety with no pneumatization of the sphenoid sinus (0%–3%).[5,7,9] In 2010, Wang et al.[15] reported the definitive classification regarding the anatomical variations of the sphenoid sinus, based on CT imaging and cadaveric specimens. To contribute to this previous work, we attempted to define a newer and perhaps more practical characterization of the neurosurgical anatomy of the sellar region, with regard to preoperative MR imaging studies and intraoperative findings during the endoscopic transsphenoidal approach. Although one limitation of our study is that MR imaging is not the optimal modality for assessing bony anatomy, it nonetheless constitutes the gold standard for imaging most sellar and parasellar lesions. Our study was intended to assess the degree to which MR findings could be correlated with the surgical anatomy. We noted that these measurements could be reliably ascertained and used in all patients to draw practical comparisons for making intraoperative predictions, especially as these predictions relate to the ability to identify and expose the sella intraoperatively and to the benefits of intraoperative neuronavigation for identification of the sellar floor. Although the presence of a prominent sella or simple sinus configuration does not obviate the usefulness of intraoperative neuronavigation, the presence of a flat sella or complex sinus configuration may suggest that the approach to and identification of key anatomical structures may be more challenging than in patients with simple sinus configurations or a prominent sella type.

Anatomy in the Sagittal Plane

According to the current study, the most common sellar morphological type (occurring in 63% of people) is a curved, intermediate type with a mean sellar angle of 116° and a mean prominence of 2.8 mm. A “prominent” sellar floor, identified in 25% of people, is associated with a longer and more convex sella, and more acute tuberculum sellae and sellar-clival angles. This type is observed to occur more frequently in patients with sellar lesions

(especially macroadenomas), is due to chronic expansion of the sella turcica, and can be identified more easily during surgical approaches. A “flat” sellar morphology, on the other hand, occurs in 11% of healthy adults, is associated with a “presellar” sphenoid sinus, a shorter and less prominent sellar face, and a flattened tuberculum sellae and sellar-clival angles; typically it requires the use of a drill or chisel for removal of the bony sellar floor.

In the current study, the mean angle of the tuberculum sellae was 112° in healthy adults. This corroborates the findings of previous radiographic studies that have reported a tuberculum sellae angle of 110°.[14] Our findings are also in agreement with previous descriptions of the sellar angle becoming more acute as expansion of intrasellar tumors occurs.[7,14] In the current study, the mean tuberculum sellae angle of patients with sellar lesions was 105°, compared with 112° in healthy adults ($p < 0.01$). Similarly, the sellar-clival angle is more acute in patients with sellar tumors (especially macroadenomas) compared with healthy adults (105° vs 117°, $p < 0.01$). Finally, no differences in any measurement parameters were noted between healthy adults and patients with microadenomas.

A significant degree of sellar expansion and thinning of the sellar floor is known to accompany the growth of sellar lesions. In lesions that erode through the sellar floor into the sphenoid sinus, identification and exposure of the sella turcica typically does not provide a challenge. In the 10% of patients with a flat sellar morphology, however, intraoperative identification of the sella may be more challenging, as these patients tend to have inconspicuous sellar floors that are less distinct from the planum sphenoidale (less-angled tuberculum sellae) and clivus (less-angled sellar-clival angle). Preoperative identification of patients with a flat sella, in addition to a presellar pneumatization pattern, may inform the surgeon that the benefits of intraoperative fluoroscopy or neuronavigation may be heightened, and the requirement for drilling or chiseling of the sellar floor is more likely. On the other hand, in patients with sellar expansion and a prominent morphological type, the sellar floor can typically be identified easily and opened by simple fracture with a nerve hook or pituitary forceps. Furthermore, varying types of sellar pathology may be expected to expand or erode the skull base to different degrees, based on lesion size, location, and biological behavior, although these factors were not analyzed as part of the current study. For instance, nonfunctional adenomas and meningiomas tend to be relatively large at the time of diagnosis, and may therefore be more likely to be associated with chronic sellar expansion than their smaller, functional adenoma counterparts. In addition to characterizing sellar floor anatomy, sagittal MR imaging can be useful in identifying tumors with a predilection for inferior extension through the sellar floor and into the sphenoid sinus and clivus (Fig. 13), especially in patients with growth-hormone–secreting adenomas and those with atypical tumors.[17] On the other hand, cystic lesions such as Rathke cleft cysts or craniopharyngiomas frequently have suprasellar components and may therefore be less likely to expand the skull base.

Anatomy in the Coronal Plane

On MR imaging studies, over 70% of people were classified as having a simple sphenoid sinus morphological type, which was substantially easier to correlate with intraoperative

findings. The remainder of patients (29.3%) had a complex sphenoid sinus pattern that created greater difficulty in locating the sellar midline and posed a greater risk of achieving subtotal exposure of the entire sellar dura; these patients benefited more from the use of intraoperative neuronavigation.

During each phase of a transsphenoidal operation, implementation of several routine practices may optimize the trajectory to the sellar midline and minimize the risk to critical paramedian neurovascular structures. Patient positioning is one critical factor that deserves particular attention prior to any transsphenoidal operation. In the majority of cases, the head is placed in 3-point fixation to use intraoperative neuronavigation. Our preference is to position the patient's head parallel to the walls of the operating room, to maximize the surgeon's sense of awareness of the midline during the approach. Superficially, the midline of the upper teeth and philtrum can be referred to as reliable midline markers during any stage of the operation, whereas the nasal septum is not a reliable midline marker as it is frequently deviated in patients, especially following any surgical manipulation. The base of the vomer and the superior sphenoid rostrum are among the most reliable midline anatomical landmarks, and can be referred to at any stage of the operation to reassess midline position (Fig. 11). Finally, during the sellar phase of an endoscopic transsphenoidal operation, a small dural filum originating from the midline sellar dura can be observed following removal of the bony sellar floor in approximately one-half of patients, and can be used a reliable indicator of the midline[16] (Fig. 14).

The identification of several bilateral structures can also be used to approximate the location of the midline, including the parasellar carotid protuberances, OCRs, clival carotid prominences, and cavernous sinus dura, following lateral exposure of the bony sellar face (Fig. 12). Although the bilateral OCRs may not be routinely observed during a standard sellar approach, and identification of these structures is not actively pursued, we found that the parasellar carotid protuberances and clival-carotid prominences more often served as bilateral markers than the OCRs. Similarly, in an anatomical study of the sphenoid sinuses performed by Wang et al.,[15] identification of a prominent unilateral OCR (pneumatized optic strut) was possible on CT images in only 21% of studies. Following bony sellar exposure, visualization of the dura overlying the cavernous sinuses and routine use of Doppler ultrasonography to assess for the underlying intercavernous ICA provide additional measures for extrapolating the location of the midline and maximize the safety profile associated with a wide opening of the sellar dura.[3]

Patients with nonpneumatized sphenoid sinuses, a majority of whom are children, require substantial consideration if a transsphenoidal approach is to be attempted[15] (Fig. 3). Identification of the midline is even more crucial during these cases, as the greater part of the approach proceeds through bone rather than through air. Visualization of bilateral structures usually identifiable within a pneumatized sphenoid sinus, such as the OCRs and carotid protuberances, is typically compromised. The use of the high-speed diamond drill for removal of cortical bone and a curette for removal of trabecular bone marrow typically maximizes the safety associated with these approaches. Intraoperative neuronavigation is recommended for all of these cases, although it in no way lessens the importance of the surgeon's knowledge of the relevant surgical anatomy.

Reoperation in patients who have undergone previous transsphenoidal surgery also deserves added consideration prior to surgery. Often, the natural anatomical landmarks that are typically used for midline orientation, such as the vomer, have been removed completely or displaced. If the prior operation was recent, the previous sellar defect can often be identified, and a prior operative corridor may facilitate the operation. Patients who had surgery several years previously, however, frequently have atypical scarring and bony overgrowth that require additional attention for correlating imaging with intraoperative anatomical features. The base of the vomer, superior attachment of the sphenoid rostrum, and parasellar carotid protuberances frequently remain intact in reoperation cases.

In comparing healthy adults, patients with smaller (< 10 mm) lesions, and those with larger (≥ 10 mm) sellar lesions, evidence of progressive sellar expansion in the medial-lateral direction was evident and correlated with the size of the lesion. The sphenoid sinus and sellar face were wider in the patients than in the healthy adults, and this widening was more pronounced in patients with larger lesions. These results corroborate previous findings relating to gradual remodeling of the bony skull base associated with longstanding, gradually expanding benign skull base tumors.[7]

In addition to bony expansion, gradual widening of the inter-ICA distance can be associated with chronic tumor growth and is a critical feature to recognize prior to performing any transsphenoidal operation (Fig. 8). The course of, and distance between, the ICAs should always be studied at multiple levels prior to surgery, especially for extended approaches requiring drilling of the clivus and tuberculum sellae or planum sphenoidale. Internal carotid arteries with dehiscent bony coverings or lateral extension into the sphenoid sinus have been reported in 4%–10% of patients, and should be screened for on preoperative imaging (Fig. 15).[4,9,10] Furthermore, “kissing” carotid arteries have been reported rarely to occur, and require additional consideration prior to selecting a transsphenoidal approach for sellar or suprasellar lesions.[8,9] In this series, the narrowest distance between parasellar ICAs noted in a patient undergoing transsphenoidal surgery was 9.1 mm, and splaying of the ICAs was noted in patients with sellar lesions compared with normal subjects. This gradual splaying was also pronounced when comparing patients with larger (≥ 10 mm) versus smaller (< 10 mm) lesions (20.2 vs 16.8 mm, $p < 0.0001$). No difference in ICA separation, however, was detected between healthy adults and patients with smaller lesions.

Conclusions

Knowledge and preoperative assessment of the normal regional anatomy and its variability are useful in predicting the intraoperative measures required to safely approach and expose the sellar region. In addition to classifying the anatomical subtype and degree of pneumatization of the sphenoid sinus, a classification scheme of sellar convexity and prominence is reported that allows surgeons to anticipate the difficulty of intraoperative identification of the sella and the potential for benefit from intraoperative neuronavigation. A prominent sella, found in 25% of people, is easier to identify during surgery, whereas 11% of people have a flat sella that is typically more difficult to identify and expose. Patients with sellar tumors, especially macroadenomas, are more likely to have prominent and convex sellar floors, consistent with chronic sellar expansion.

Although the majority of people have simple sphenoid sinus morphology that is easy to correlate with preoperative imaging studies, approximately 30% of patients have complex sphenoid sinus anatomy that makes intra-operative correlation substantially more challenging. In patients with sellar-region lesions, chronic skull base expansion of the sellar floor and widening of the parasellar ICAs is evident on preoperative MR imaging studies, and is crucial to note to avoid injury to these structures. Identification of several midline and bilateral anatomical landmarks can be used to facilitate an optimal midline trajectory during transsphenoidal and extended endonasal skull base approaches, thus minimizing the risk to critical paramedian structures.

Abbreviations used in this paper

ICA	internal carotid artery
OCR	opticocarotid recess

References

1. Cappabianca P, Cavallo LM, de Divitiis E. Endoscopic endonasal transsphenoidal surgery. Neurosurgery. 2004; 55:933–941. [PubMed: 15458602]
2. Cavallo LM, de Divitiis O, Aydin S, Messina A, Esposito F, Iaconetta G, et al. Extended endoscopic endonasal transsphenoidal approach to the suprasellar area: anatomic considerations—part 1. Neurosurgery. 2008; 62(6 Suppl 3):1202–1212. [PubMed: 18695541]
3. Dusick JR, Esposito F, Malkasian D, Kelly DF. Avoidance of carotid artery injuries in transsphenoidal surgery with the Doppler probe and micro-hook blades. Neurosurgery. 2007; 60(4 Suppl 2):322–329. [PubMed: 17415170]
4. Fujii K, Chambers SM, Rhoton AL Jr. Neurovascular relationships of the sphenoid sinus. A microsurgical study. J Neurosurg. 1979; 50:31–39. [PubMed: 758376]
5. Hamberger CA, Hammer G, Marcusson G. Experiences in transantrosphenoidal hypophysectomy. Trans Pac Coast Otoophthalmol Soc Annu Meet. 1961; 42:273–286. [PubMed: 13904062]
6. Liu JK, Das K, Weiss MH, Laws ER Jr, Couldwell WT. The history and evolution of transsphenoidal surgery. J Neurosurg. 2001; 95:1083–1096. [PubMed: 11765830]
7. Ouaknine GE, Hardy J. Microsurgical anatomy of the pituitary gland and the sellar region. 2. The bony structures. Am Surg. 1987; 53:291–297. [PubMed: 3579041]
8. Pereira Filho Ade A, Gobbato PL, Pereira Filho Gde A, Silva SB, Kraemer JL. Intracranial intrasellar kissing carotid arteries: case report. Arq Neuropsiquiatr. 2007; 65(2A):355–357. [PubMed: 17607445]
9. Renn WH, Rhoton AL Jr. Microsurgical anatomy of the sellar region. J Neurosurg. 1975; 43:288–298. [PubMed: 1151464]
10. Rhoton AL Jr. The sellar region. Neurosurgery. 2002; 51(4 Suppl):S335–S374. [PubMed: 12234453]
11. Rhoton AL Jr, Hardy DG, Chambers SM. Microsurgical anatomy and dissection of the sphenoid bone, cavernous sinus and sellar region. Surg Neurol. 1979; 12:63–104. [PubMed: 451866]
12. Schloffer H. Erfolgreiche operation eines hypophysentumors auf nasalem Wege. Wien Klin Wochenschr. 1907; 20:621–624.
13. Sethi DS, Stanley RE, Pillay PK. Endoscopic anatomy of the sphenoid sinus and sella turcica. J Laryngol Otol. 1995; 109:951–955. [PubMed: 7499947]
14. Vezina JL, Sutton TJ. Prolactin-secreting pituitary microadenomas: roentgenologic diagnosis. Am J Roentgenol Radium Ther Nucl Med. 1974; 120:46–54.
15. Wang J, Bidari S, Inoue K, Yang H, Rhoton A Jr. Extensions of the sphenoid sinus: a new classification. Neurosurgery. 2010; 66:797–816. [PubMed: 20305499]

16. Zada G, Kim AH, Governale LS, Laws ER. Midline filum of the sellar dura: a useful landmark during endoscopic transsphenoidal pituitary surgery. Neurosurgery. 2010; 67:391–394. (2 Suppl Operative). [PubMed: 21099563]

17. Zada G, Lin N, Laws ER Jr. Patterns of extrasellar extension in growth hormone–secreting and nonfunctional pituitary macroadenomas. Neurosurg Focus. 2010; 29(4):E4. [PubMed: 20887129]

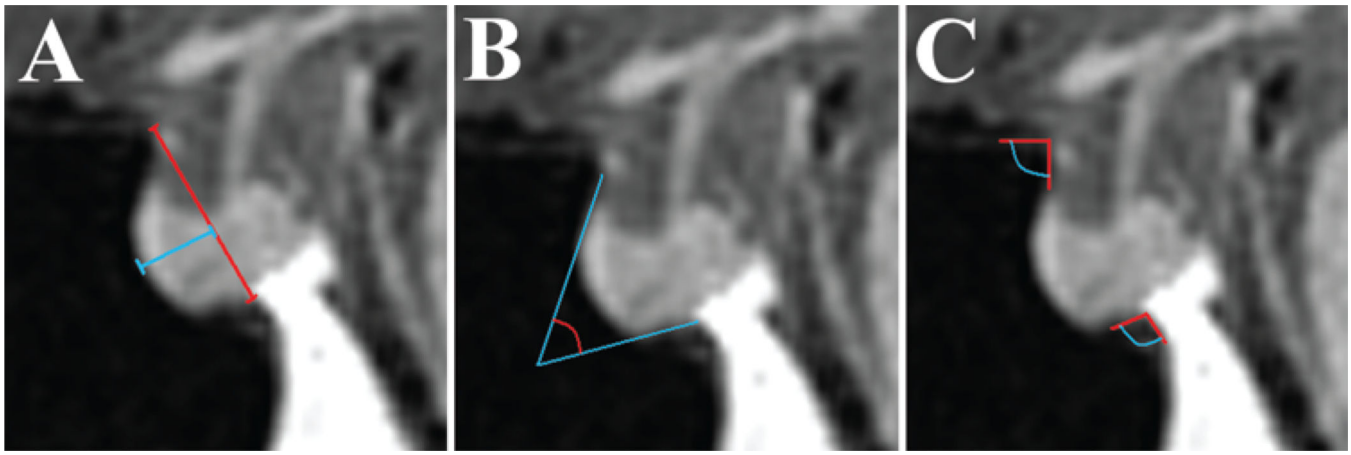

Fig. 1.

Measurements obtained on midsagittal MR images of the sella turcica. **A:** The sellar face length was defined by a line from the tuberculum sellae to the sellar-clival angle (*red line*). The prominence of the sella was defined as the maximal length from the sellar face line to the most prominent point on the sellar floor (*blue line*). **B:** Method of obtaining the sellar angle. **C:** Depicts angle measurements of the tuberculum sellae angle and sellar-clival angle.

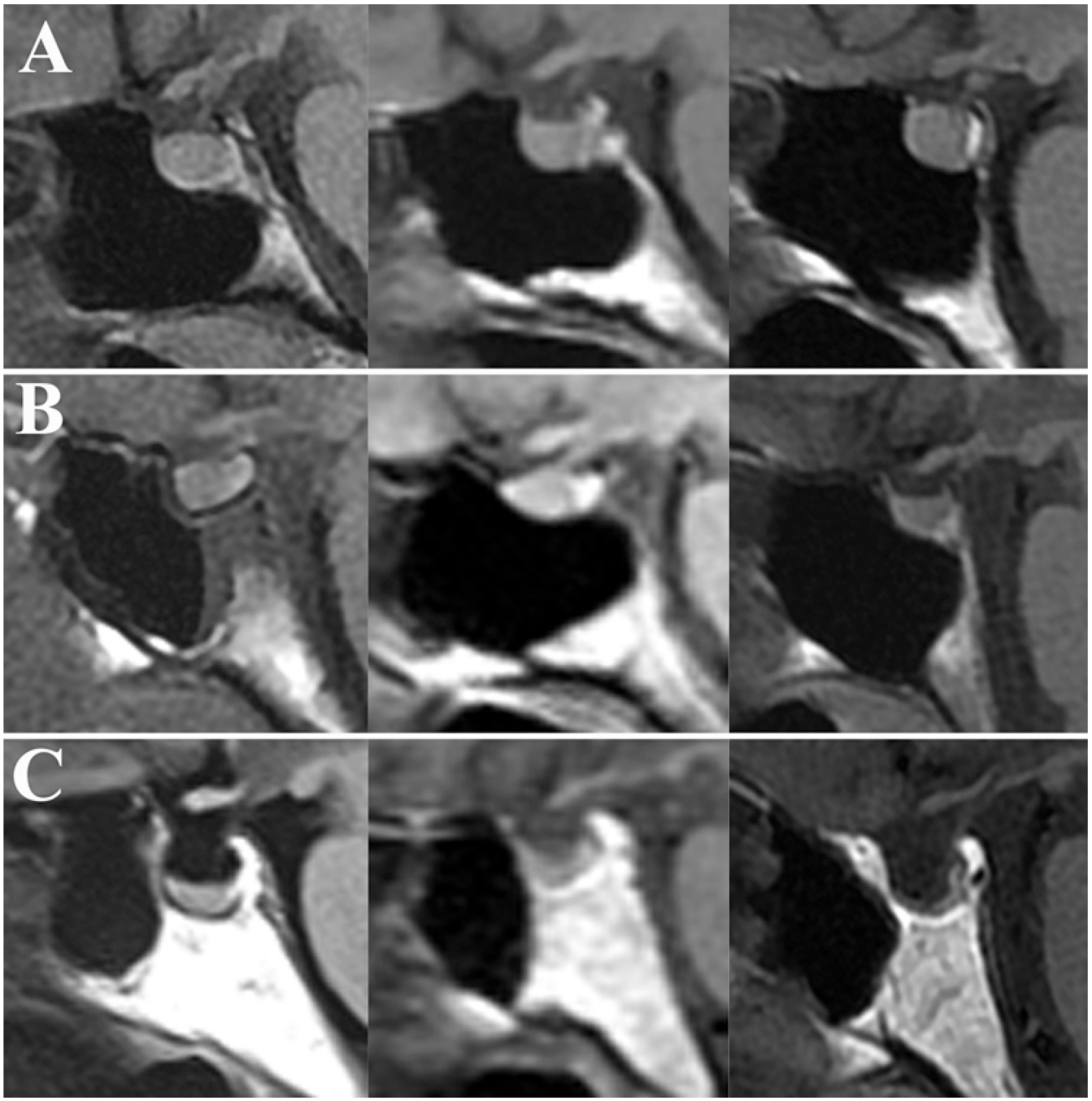

Fig. 2.

Sagittal MR images demonstrating the wide variability of sellar floor morphology in healthy adults. **A:** Representative example of the “prominent” sellar type (sellar angle < 90°) identified in 25% of individuals. **B:** Example of the intermediate “curved” sellar type (sellar angle 90°–150°) identified in 63% of individuals. **C:** Example of the less conspicuous “flat” sellar type (sellar angle > 150°) identified in 11% of individuals and often associated with a presellar sphenoid sinus.

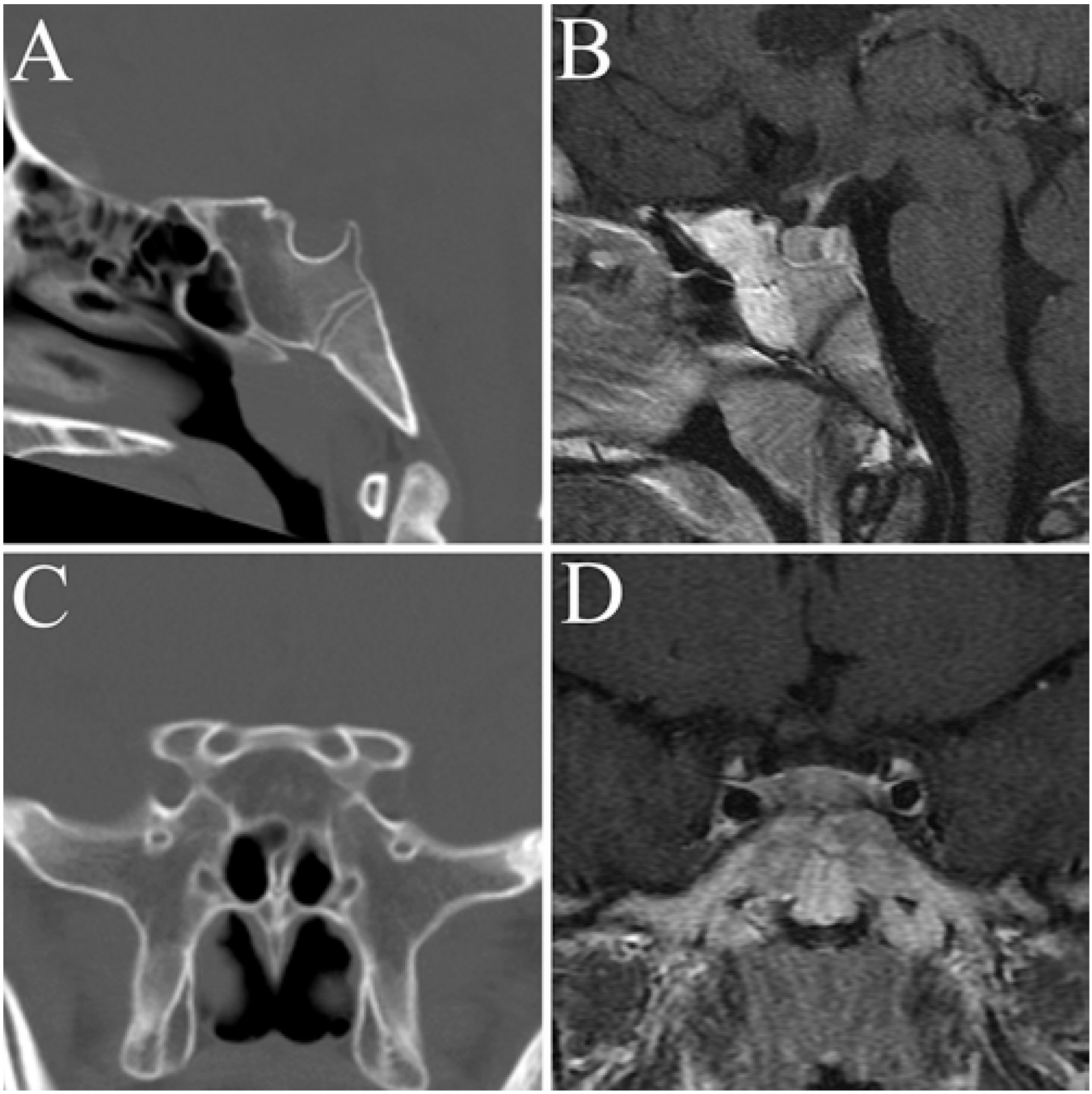

Fig. 3.

Sagittal **(A and B)** and coronal **(C and D)** CT **(A and C)** and MR **(B and D)** images showing an example of a “conchal,” or nonpneumatized, sphenoid sinus. This variation was identified in 1% of normal subjects and in no patients with sellar tumors.

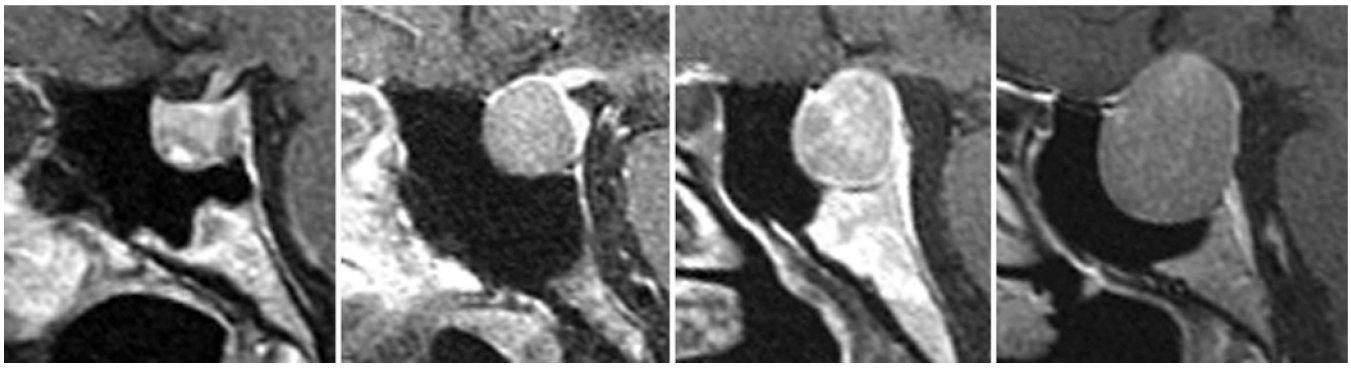

Fig. 4.

Examples of MR images obtained in obtained in patients with sellar masses and a prominent sellar type (43% of tumor patients), likely due in part to sellar expansion.

Fig. 5.

Examples of MR images obtained in patients with sellar masses and a flat sellar type (10% of tumor patients). In general, the floor of the sella associated with this morphological type is more difficult to identify intraoperatively and has a tendency to be thicker. **A–C:** Images demonstrating a flat sella in association with a presellar sinus. **D:** Image demonstrating a flat sellar face with no presellar sphenoid sinus. Without careful consideration, the sellar-clival angle could be mistaken for the tuberculum sellae in such a situation.

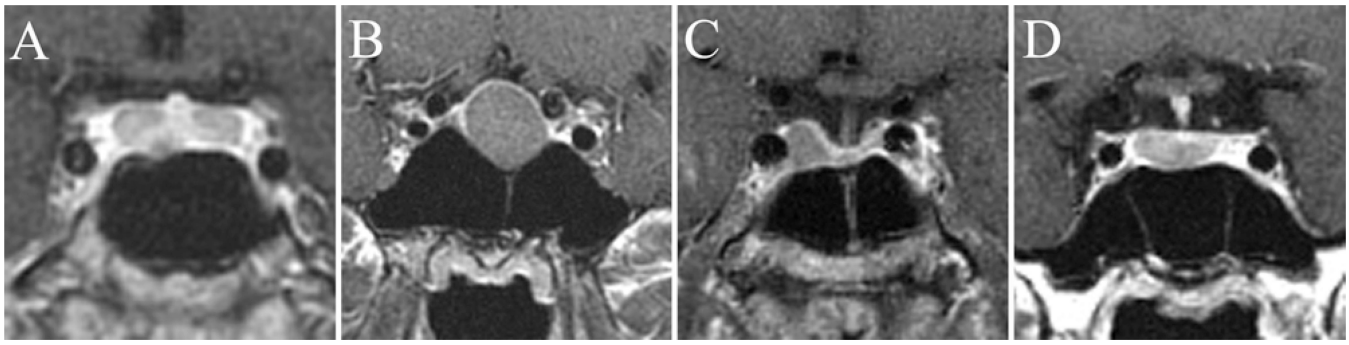

Fig. 6.

Coronal, postcontrast MR images obtained in patients with sella-based lesions and a simple sphenoid sinus morphological type. Various subtypes represented in this category include no vertical septations **(A)**, 1 midline vertical septum **(B)**, 1 slightly eccentric septum **(C)**, and 2 vertical septa creating a symmetric tripartite sinus **(D)**.

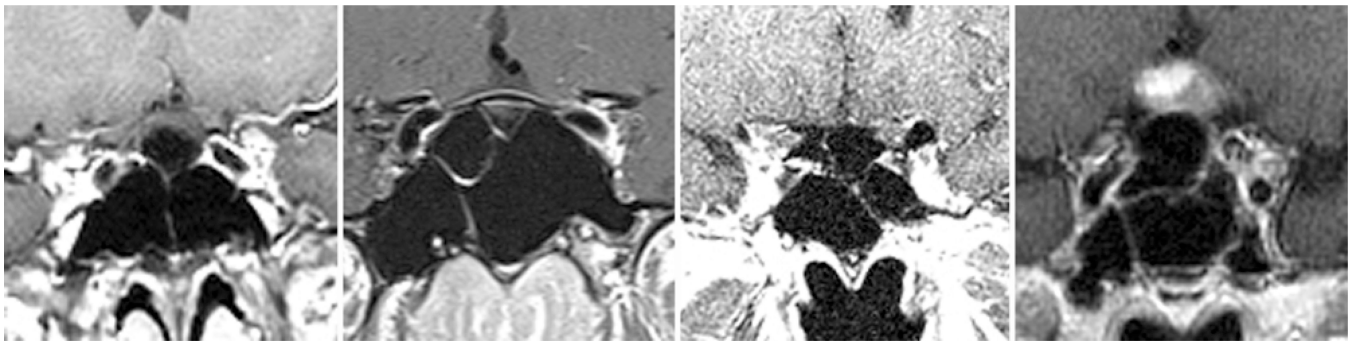

Fig. 7.

Coronal, postcontrast MR images obtained in patients with sella-based lesions and a complex sphenoid sinus morphology. These patients had more than 2 vertical septations or a combination of horizontal and vertical septa.

Fig. 8.

Examples of variation in the distance between the parasellar ICAs associated with tumor size. The inter-ICA distances in these images are 9 mm **(A)**, 16 mm **(B)**, and 25 mm **(C)**.

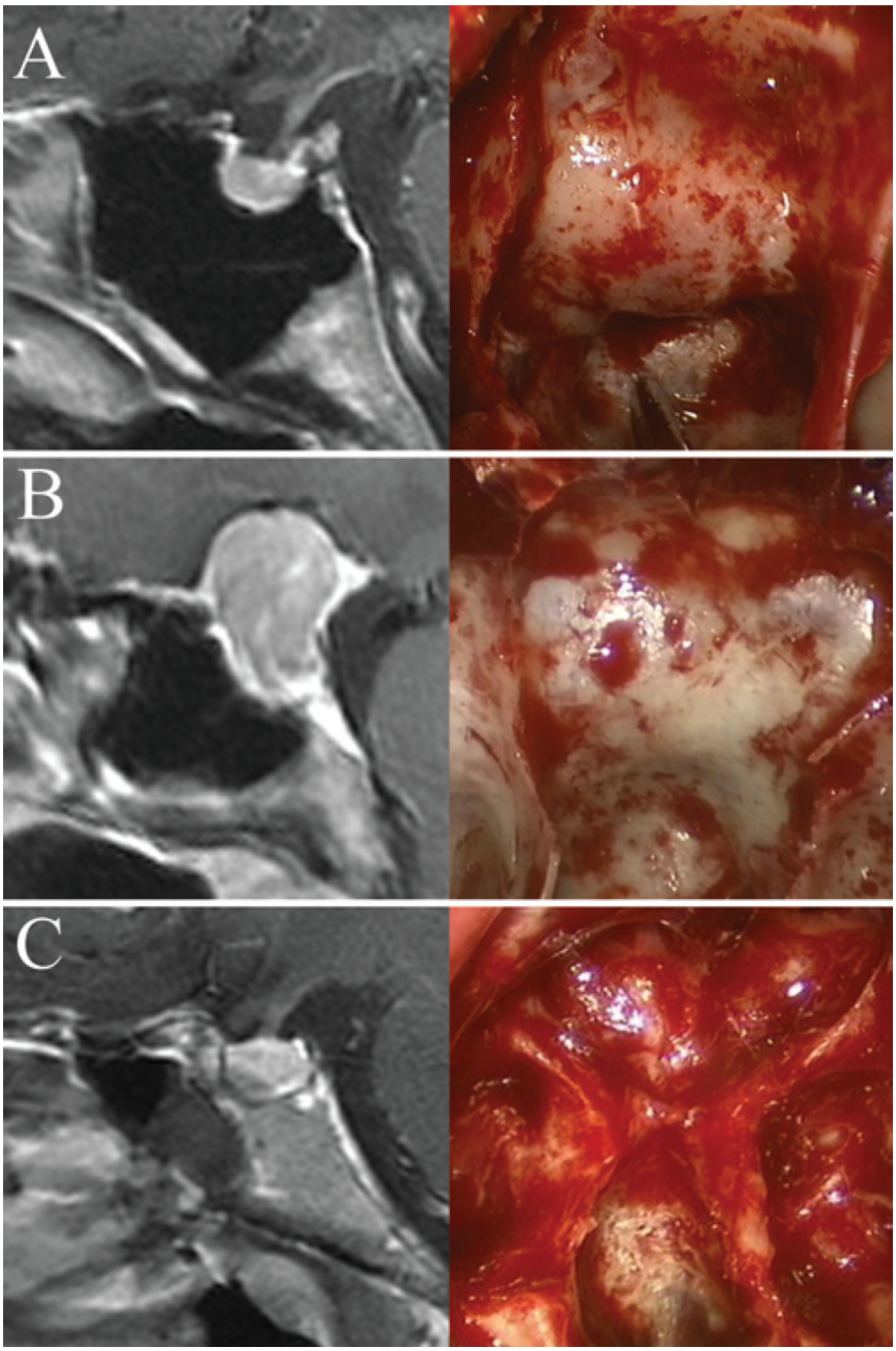

Fig. 9.

Sagittal MR imaging and intraoperative endoscopic images of the sellar floor and morphology. **A:** Example of a prominent sella that is easily identifiable intraoperatively. **B:** Example of an intermediate sellar type. **C:** Example of a flat sella that is very difficult to differentiate from the clivus. Intraoperative neuronavigation was extremely useful in this case.

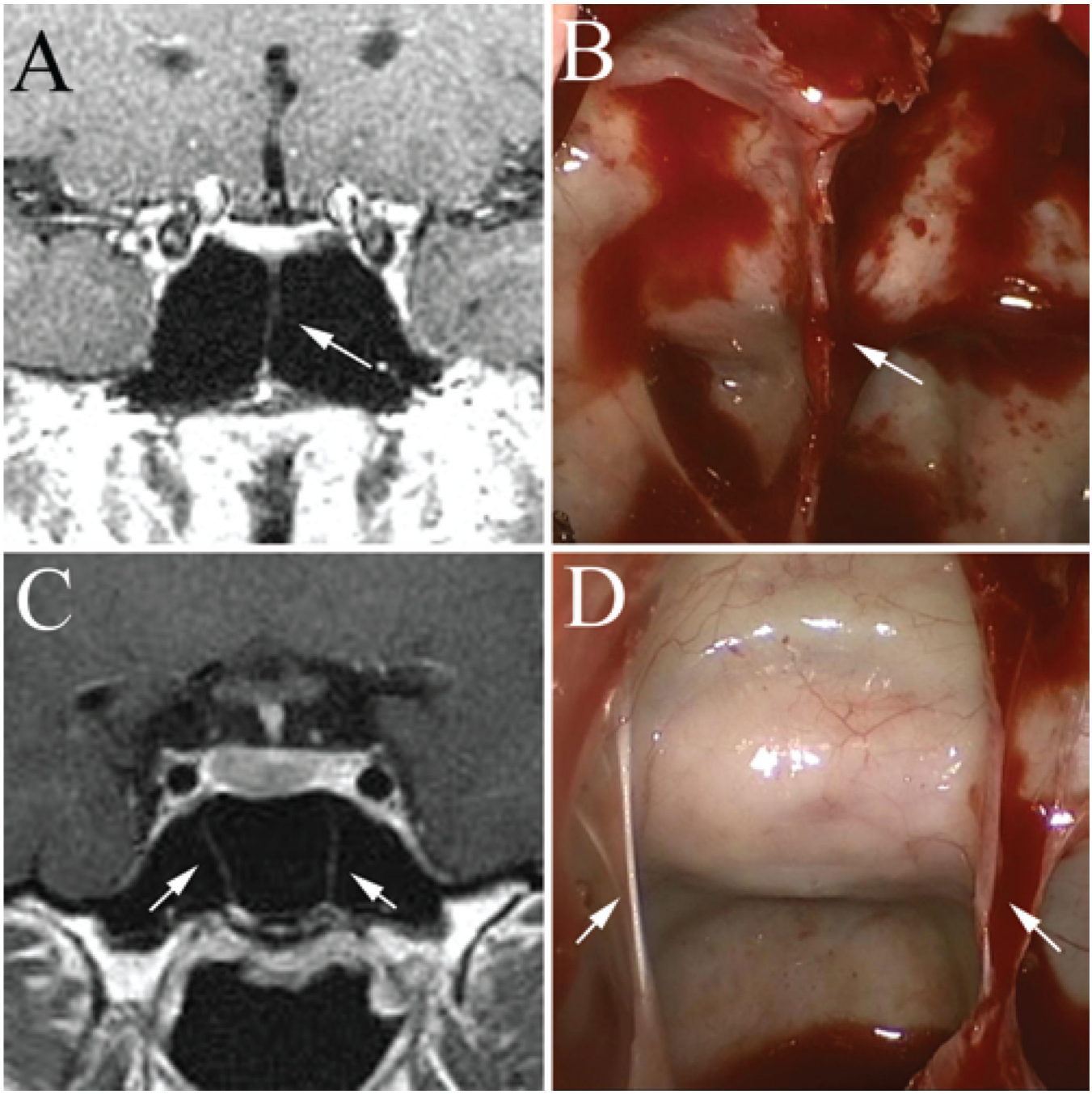

Fig. 10.

Examples of intraoperative findings–imaging correlation of vertical septa in patients with simple sphenoid sinus morphology. The presence of 1 midline vertical septum (**A and B**, *white arrow*) can be used to identify the anatomical midline. The presence of 2 symmetric vertical septa (**C and D**, *white arrows*) can typically be used to identify the lateral boundaries of the sellar exposure and extrapolate the midline location.

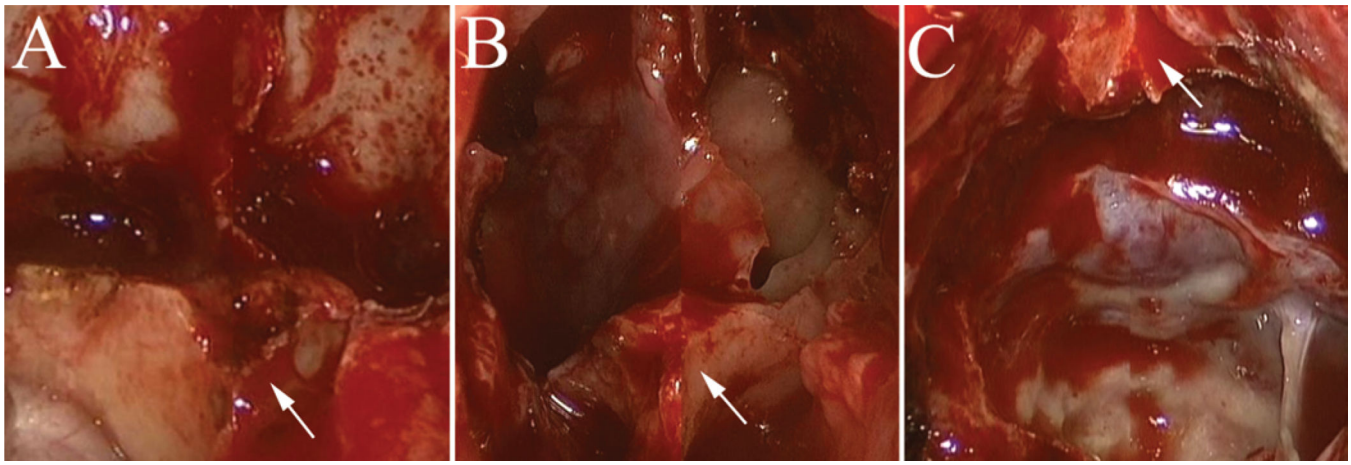

Fig. 11.

Intraoperative endoscopic photographs demonstrating the benefit of relatively constant midline markers, such as the base of the vomer (**A and B**, *white arrows*) or superior rostrum of the sphenoid (**C**, *white arrow*). These anatomical structures tend to be reliable midline markers despite the presence of eccentric sphenoid sinus septa **(B)**.

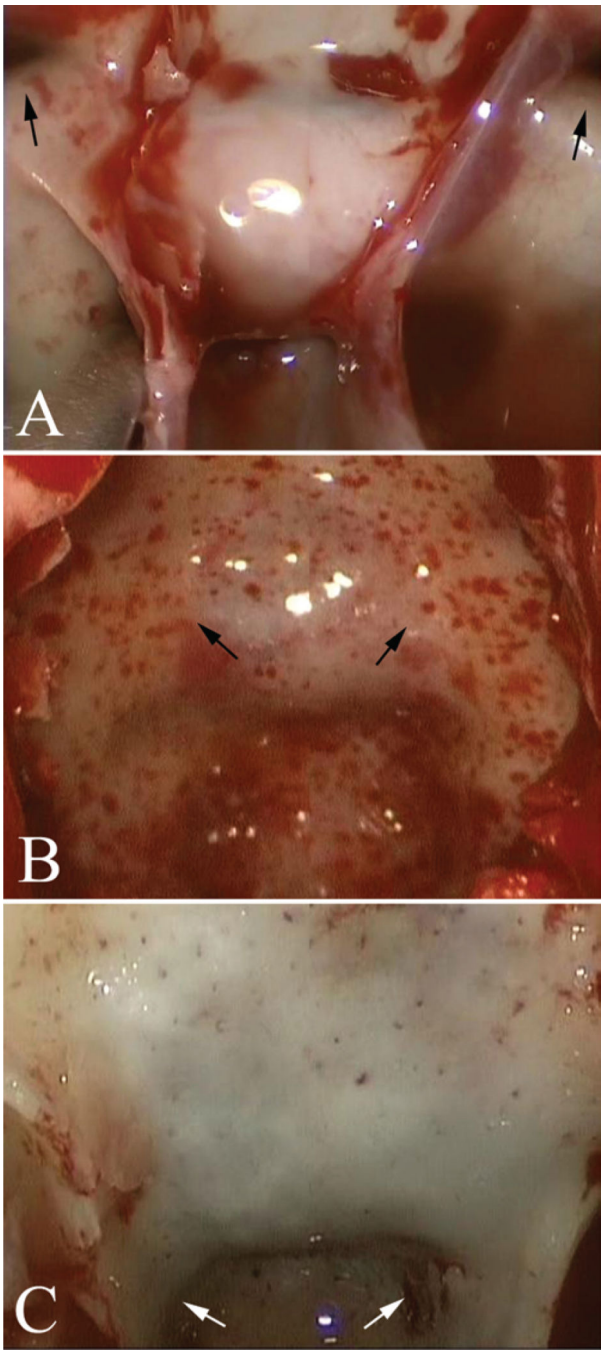

Fig. 12.

Intraoperative endoscopic photographs demonstrating the benefit of bilateral anatomical markers, including the OCRs (**A**, *black arrows*), carotid protuberances (**B**, *black arrows*), and clival-carotid prominences (**C**, *white arrows*). Note the prominent sellar curvature in **B** that substantially facilitates intraoperative identification.

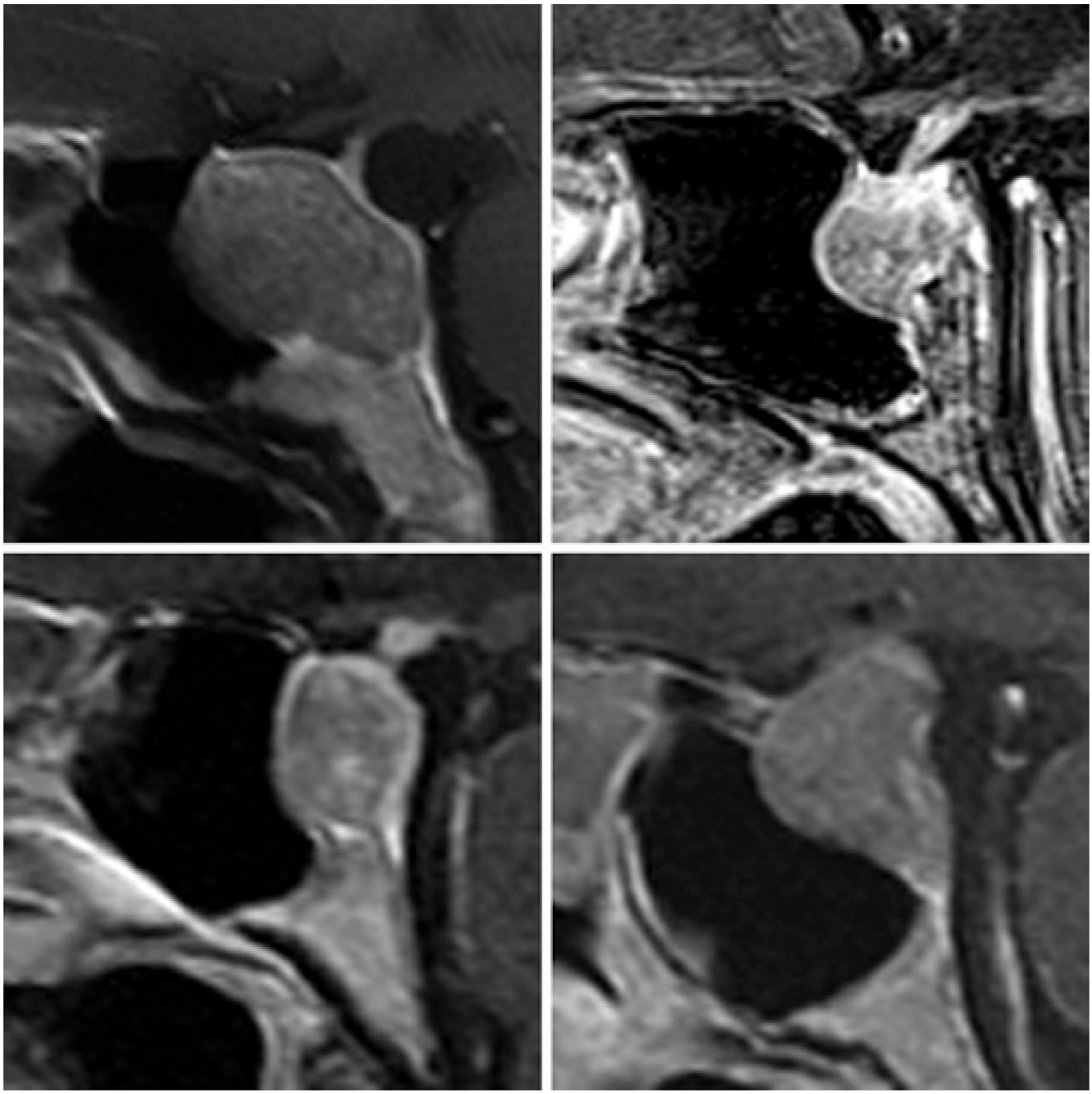

Fig. 13.
Sagittal MR images obtained in 4 patients with pituitary adenomas and clival erosion without obvious erosion of the sellar floor.

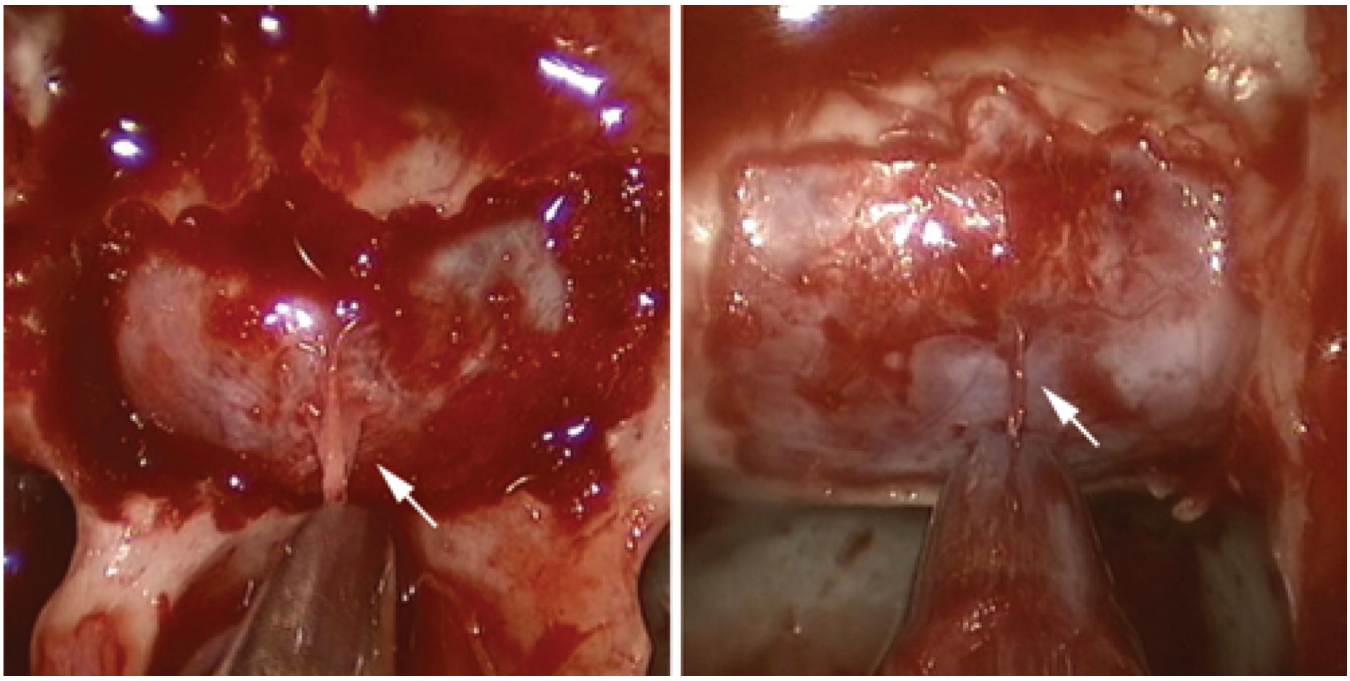

Fig. 14.

Intraoperative endoscopic photographs during the sellar phase of a transsphenoidal operation following removal of the bony sellar floor. In approximately one-half of patients, a midline dural filum (*white arrows*) is noted that correlates with the midline.

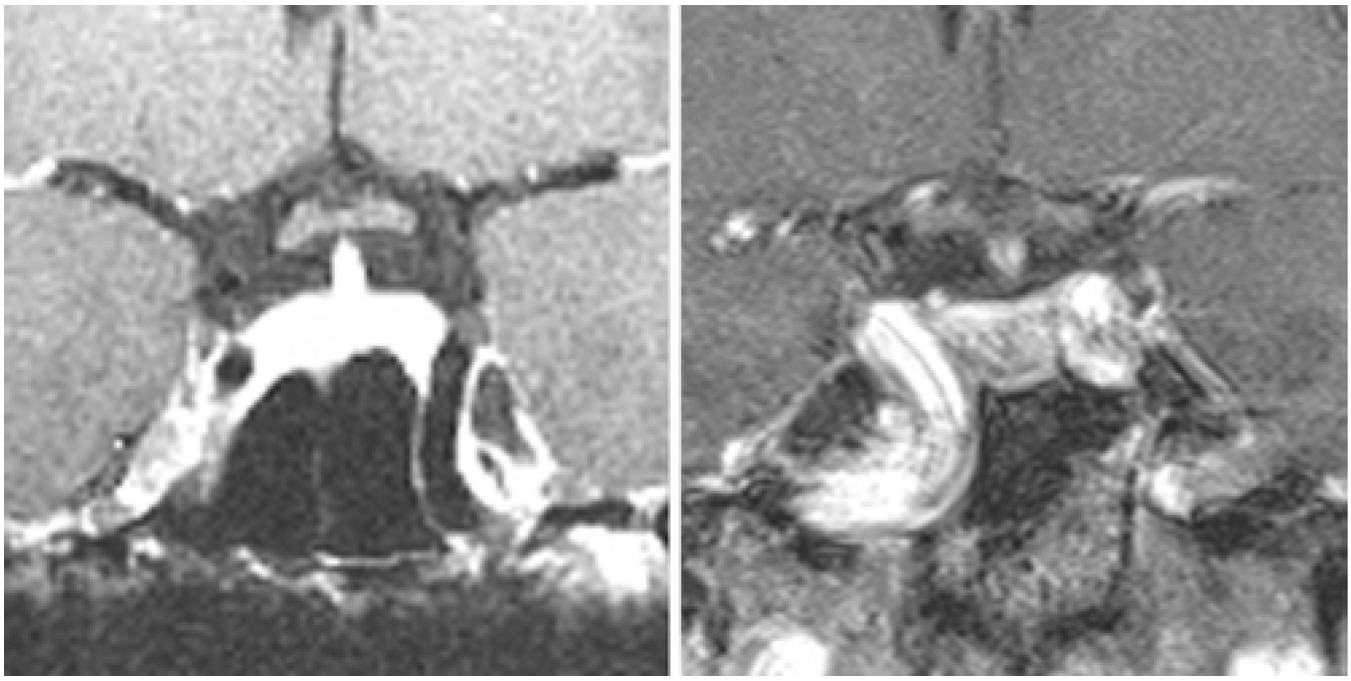

Fig. 15.

Coronal, postcontrast MR images obtained in 2 patients with prominent ICA projection into the sphenoid sinus (present in 4%–10% of patients), warranting additional caution during the sphenoid phase of a transsphenoidal operation.

TABLE 1

Mean measurements of the sellar floor and sphenoid sinus in 100 healthy adults, grouped according to sellar type

Sellar Type	No. of Individuals (%)	Sellar Face (mm)	Sellar Prominence (mm)	Planum Sphenoidale Length (mm)	Clivus Length (mm)	Sellar Angle (°)	Tuberculum Sellae Angle (°)	Sellar-Clival Angle (°)
prominent (<90°)	25 (25)	14.7	4.6	15.3	16.6	80	103	101
curved (90°–150°)	63 (63)	13.1	2.8	13.9	14.1	116	115	119
flat (>150°)	11 (11)	12.0	0.6	11.9	12.6	163	113	143
conchal	1 (1)							
all	100 (100)	13.4	3.0	14.1	14.6	112	112	117

TABLE 2

Mean sellar floor measurements in healthy adults, all tumor patients, and macroadenoma patients*

Measurement	Healthy Adults	All Tumor Pts	p Value	Macroadenoma Pts	p Value
sellar face (mm)	13.4	15.4	<0.0001	16.5	<0.0001
sellar prominence (mm)	3.0	3.8	0.0036	4.2	0.0002
planum sphenoidale length (mm)	14.1	13.9	0.87	13.3	0.3042
clivus length (mm)	14.6	14.2	0.55	14.2	0.63
sellar angle (°)	112	102	0.0326	99	0.0095
tuberculum sellae angle (°)	112	105	0.0058	103	0.0011
sellar-clival angle (°)	117	105	0.0026	103	0.0011

* For statistical analysis, macroadenoma patients were compared with healthy adults.

Abbreviation: Pts = Patients.

TABLE 3

Sellar type in healthy adults and patients with sellar lesions*

	No. of Individuals (%)			
Sellar Type	**Healthy Adults**	**All Tumor Pts**	**Microadenoma Pts**	**Macroadenoma Pts**
prominent (<90°)	25 (25)	33 (43)	8 (35)	25 (45)
curved (90°–150°)	63 (63)	37 (47)	12 (52)	25 (45)
flat (>150°)	11 (11)	8 (10)	3 (13)	5 (10)
total	100 (100)	78 (100)	23 (100)	55 (100)

* Patients with sellar tumors were more likely to have prominent sellae than were heathy adults ($p = 0.0163$); the same was true for patients with macroadenomas ($p = 0.0119$). No statistically significant difference was observed between microadenoma patients and healthy adults.

TABLE 4

Classification of sphenoid sinus septum morphology and complexity based on coronal MR imaging in 178 individuals*

Morphological Type (% of studies)	No. of Septa	Orientation of Septa	Position/Symmetry	No. of Studies (%)
simple (70.7)	0	NA	NA	16 (9.0)
	1	vertical	midline/symmetric	33 (18.5)
	1	vertical	eccentric/asymmetric	61 (34.2)
	2	vertical	tripartite/symmetric	16 (9.0)
Complex (29.3)	1	horizontal	any	1 (0.6)
	2	vertical	asymmetric	24 (13.5)
	2	horizontal + vertical	any	17 (9.6)
	≥3	any	any	10 (5.6)
total				178 (100)

* 100 healthy adults and 78 patients with sellar tumors.

TABLE 5

Measurements based on coronal MR imaging in healthy adults and in patients with sella-based lesions

Variable	Healthy Adults	All Pts w/ Sellar Lesions	p Value
max sinus width (mm)	30.1	31.4	0.047*
sellar face width (mm)	12.7	15.9	<0.0001*
inter-ICA distance (mm)			
parasellar	16.2	19.0	<0.0001*
midclivus	18.5	18.1	0.25

*Statistically significant.

TABLE 6

Measurements based on coronal MR imaging in healthy adults and in patients with sella-based lesions measuring less than 10 mm in maximum diameter*

Variable	Healthy Adults	Pts w/ Sellar Lesions <10 mm	p Value
max sinus width (mm)	30.1	29.2	0.29
sellar face width (mm)	12.7	14.2	0.0008*
inter-ICA distance (mm)			
parasellar	16.2	16.8	0.42
midclivus	18.5	17.9	0.22

*Statistically significant.

TABLE 7

Measurements based on coronal MR imaging in patients with sella-based lesions measuring less than 10 mm in maximum diameter versus those measuring 10 mm or greater

	Mean Value		
Variable	**Pts w/ Sellar Lesions <10 mm**	**Pts w/ Sellar Lesions ≥10 mm**	**p Value**
max sinus width (mm)	29.2	32.7	0.0012*
sellar face width (mm)	14.2	16.8	<0.0001*
inter-ICA distance (mm)			
parasellar	16.8	20.2	<0.0001*
midclivus	17.9	18.2	0.63

*Statistically significant.

TABLE 8

Method of exposure of the sellar floor in patients with 3 sellar types*

	No. of Cases (%)	
Sellar Type	**Fractured**	**Chisel or Drill**
prominent	21 (75)	7 (25)
curved	22 (61)	14 (39)
flat	2 (25)	6 (75)

* Exposure was more likely to require a chisel or drill in patients with the flat sellar type than in patients with prominent floors ($p = 0.0157$).